STAFF SUMMARY SHEET

	TO	ACTION	SIGNATURE (Surname), GRADE AND DATE		TO	ACTION	SIGNATURE (Surname), GRADE AND DATE
1	DFAN	sig	REED SHAD LT COL 25NOV14	6			
2	DFER	approve	SCOTT, AD 25, 1 Dec 14	7			
3	DFAN	action	(Author /Originator)	8			
4				9			
5				10			

SURNAME OF ACTION OFFICER AND GRADE	SYMBOL	PHONE	TYPIST'S INITIALS	SUSPENSE DATE
McLaughlin, CIV		333-2613	jmi	20141126

SUBJECT		DATE
Clearance for Material for Public Release	USAFA-DF-PA- 503	20141124

SUMMARY

1. PURPOSE. To provide security and policy review on the document at Tab 1 prior to release to the public.

2. BACKGROUND.
Authors: Casey Fagley, Jurgen Seidel and Thomas McLaughlin

Title: Investigation of Aeroelastic Flow Control of a FlutteringWing with HPCMP CREATE™-AV Kestrel

Circle one: Abstract Tech Report Journal Article Speech Paper Presentation Poster

Thesis/Dissertation Book Other: _____

Check all that apply (For Communications Purposes):

[x] CRADA (Cooperative Research and Development Agreement) exists

[] Photo/ Video Opportunities [] STEM-outreach Related [] New Invention/ Discovery/ Patent

Description: This conference paper computationally investigates fluid-structure interaction of a torsionally flexible wing with and without the use of flow control via blowing ports.

Release Information: This work is funded by the Air Force Office of Scientific Research

Previous Clearance information: None

Recommended Distribution Statement: Distribution A: approved for public release, distribution unlimited

3. DISCUSSION.

4. RECOMMENDATION. Sign Coord block above indicating document is suitable for public release. Sutiability is based solely on the document being uunclassified, not jeopardizing DoD interests, and accurately portraying official policy.

THOMAS E. MCLAUGHLIN, Ph.D.
Director, Aeronautics Research Center

Investigation of Aeroelastic Flow Control of a Fluttering Wing with HPCMP CREATE™-AV Kestrel

Casey Fagley*, Jürgen Seidel†, Thomas McLaughlin‡
Department of Aeronautics, U.S. Air Force Academy, CO 80840, USA

The aeroelastic behavior of a finite aspect ratio ($\mathcal{AR}$= 6) NACA0018 wing is computationally analyzed. HPCMP CREATE™-AV Kestrel, a fully coupled computational fluid dynamic (CFD) and computational structural dynamic (CSD) code, is used to compare the effect of blowing on a rigid and an aeroelastically deforming wing. Externally controlled blowing slots distributed along the span of the wing are used to inject mass into the flow field to achieve open-loop flow control. The results indicate that control by blowing has a pronounced effect on the flowfield and therefore on the aerodynamic coefficients. For the rigid wing, the lift is increased, as are the pitching and rolling moments. When aeroelastic deformation is considered, the picture changes significantly. First, the flexible wing showed higher lift and drag compared to the rigid wing due to the increased local angle of attack in the outboard section of the wing. Furthermore, the pitching and rolling moments were significantly reduced.

Nomenclature

A_{jet}	Jet orifice area	$\mathbf{q}$	Structural displacement
A_{ref}	Reference area	s	Laplace variable
b	Span	U_∞	Freestream velocity
$\mathbf{C}$	Damping matrix	$\hat{V}$	Jet velocity vector
c	Chord	V_{jet}	Jet velocity magnitude
C_D	Drag coefficient	α	Angle of attack
C_L	Lift coefficient	λ	Eigenvalue
C_μ	Momentum coefficient	ϕ	Eigenvector
$\mathbf{K}$	Stiffness matrix	ρ	Density
$\mathbf{M}$	Mass matrix	$\mathcal{AR}$	Aspect ratio
$\hat{n}$	Normal vector		

I. Introduction

AEROELASTICITY is a very well studied scientific field combining structural dynamics, aerodynamics and interactions thereof. Typically, aeroelasticity is represented by Collars triangle of forces which shows the interplay between forces present in an aeroelastic system. A simplified triangle of forces is depicted in Figure 1.

The transfer of energy between inertial, elastic, and aerodynamic forces produces a potentially unsteady aeroelastic behavior. This unsteady fluid-structure interaction is a prominent design consideration for current air vehicles; for instance, at certain operating conditions (i.e. Mach number, altitude, fuel levels, cargo weight, etc.) aeroelastic instabilities may be present and be detrimental to the aircraft structure. This instability is typically identified as flutter, or, in the situation of a marginally stable system, a limit cycle oscillation. Aircraft design needs to maintain a reasonable safety margin from any aeroelastic instability; therefore, a wide variety of methods exist to predict flutter margins [1–4]. Each of these methods have one unified goal which is to identify the true damping of the aero-structure system. This damping gives the stability criterion as a function of operating condition (mainly Mach number and altitude). Current aircraft designs are pushing these stability margins to achieve lighter weight and therefore more

*Research Associate, Department of Aeronautics, Member, casey.fagley@usafa.edu
†Research Associate, Department of Aeronautics, Senior Member
‡Director, Aeronautics Research Center, Department of Aeronautics, Associate Fellow

efficient flight vehicles; thus, the need to understand the source of these aeroelastic instabilities and potentially be able to suppress the instability on order to expand the flight envelope is greater than ever.

The typical approach to suppressing aeroelastic instabilities is by using control surfaces, i.e. flaps or ailerons, to counter act unsteady aerodynamic loads due to structural displacements. In terms of actuation most, if not all, active aeroelastic control endeavors utilize a conventional trailing edge flap to alter the aerodynamics. For instance, in the case of the design of the X-56A, a NASA designed Multi-Utility Technology Testbed for flutter suppression techniques, the trailing edge flap actuator bandwidth was 10 Hz [5] and the flutter instabilities were on the order of 5-15 Hz [6]. Alternatively, sensors such as accelerometers and strain gauges have long been the conventional devices of choice to instantaneously measure the wing deformation. Both sensors rely upon the structural deformation for sensing of the aeroelastic phenomena. The bandwidth demand for flutter suppression is a huge concern for the stability and robustness of the control system and, ultimately, leads to the motivation of this work: to employ active flow control to augment the local flow features to suppress aeroelastic instabilities.

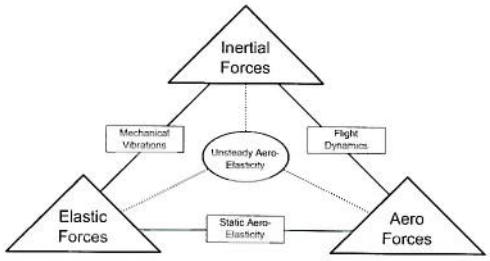

Figure 1. Modified Collar's triangle representing the forces at play in an aeroelastic system.

Active flow control, which introduces a small amount of energy to the flow (e.g. by blowing fluid into the main flow), allows for direct, local, and instantaneous modification of the flow field. The perturbation of the flow is amplified through a natural fluidic instability which affects the global flow state. Thus, the control effort remains small by exploiting the fluidic instability and the bandwidth of the system is equivalent to the convective frequency of the flow [7]. In the past, both passive and active (including open- and closed-loop) flow control techniques have been exhaustively studied (see review articles, e.g. [8, 9]), but upon a survey of the literature, implementation of active closed-loop flow control to real-life applications has largely eluded the research and engineering communities to date [9]. The development of a functioning control system for a range of flow conditions has proven to be a formidable challenge.

The research presented in this paper utilizes Kestrel, a fully coupled computational fluid dynamic (CFD) and computational structural dynamic (CSD) code, to assess the aeroelastic behavior of a generic wing. Externally controlled mass injection slots are used to augment local flow features, and the global response is characterized. It is shown through these high fidelity simulations that flow control on aeroelastically deforming surfaces is possible. Also, a flow field analysis is performed and interesting relationships between forcing and structural responses are obtained.

II. Setup

Simulations were performed on a cantilevered, rectangular, flexible NACA0018 wing with a span of $b = 0.6$m, a chord of $c = 0.1$m, and an aspect ratio of AR=6. The geometry is shown in Fig. 2; note that the origin of the coordinate system is at the root leading edge, with the x-axis pointing downstream, the y-axis in the spanwise direction, and the z-axis upward.

Four rectangular blowing slots were integrated on the upper surface near the leading edge of the wing. The slots were placed in 1/2 chord increments from the tip toward the root of the wing. The slot dimensions are 1mm by 10mm. The orientation of the slots was chosen to be angled upward by 30° with the slot blowing surface on the chord line at the 10% chord. The slot location and geometry are also shown in Fig. 2(bottom). Since the slots were placed in an area of a favorable pressure gradient, it is expected that the effect forcing the flow by blowing out through the slots will be most effective at large angles of twist (i.e., large local angles of attack) where the flow is close to separation near the leading edge.

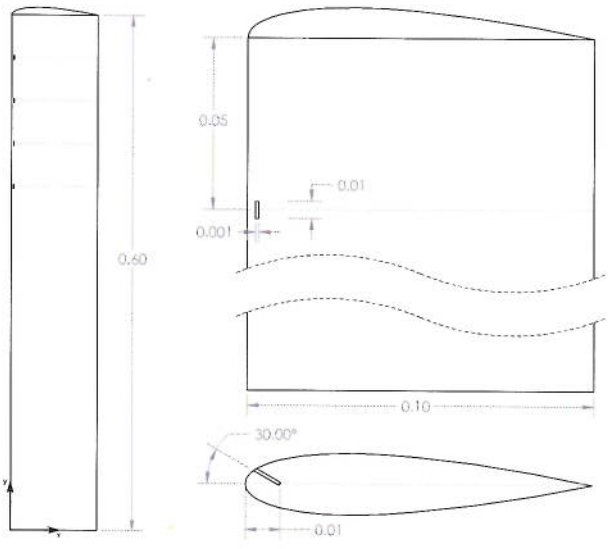

Figure 2. NACA0018 geometry and blowing slot configuration.

The free stream velocity was set to $U_\infty = 34$m/s, cor-

responding to a Mach number of $M = 0.1$. The chord based Reynolds number is $Re_c = 160,000$ and the angle of attack was set to $\alpha = 6\,\text{deg}$.

A. Coupled Aeroelastic CFD

The HPCMP CREATE™-AV Kestrel software suite was employed for the simulations in this research. The software suite is designed to allow for development of extensions such as a flow control component. [10–13] The underlying program structure is based upon an event based model, where the various components in the simulation subscribe to and trigger events. This architecture allows for great flexibility of simulations without sacrificing performance.

Kestrel is based on the AVUS flow solver developed at the Air Force Research Laboratory at Wright-Patterson Air Force Base. It is a multidisciplinary, second-order in space and time, cell-centered, finite-volume Navier-Stokes solver for grids with arbitrary cell topologies. Kestrel features different flux schemes, limiters and turbulence models. Aeroelastic analysis, moving control surfaces, overset grids and rigid-body motions are some of the features in the current version of Kestrel.

Kestrel v5.1 features a number of turbulence models, including Spalart-Allmaras(SA) [14], Spalart-Allmaras with rotation correction (SARC) [15], Menter's model (Menter) [16], and Menter's shear stress transport (SST) [16]; all RANS models can be operated in Delayed Detached-Eddy Simulation (DDES) [17] mode to provide hybrid RANS/LES (Large Eddy Simulation) simulation capability. The simulations presented in this paper were performed using the DDES approach with the SA turbulence model.

To accomplish the final research goal of this project, namely feedback flow control of a flexible wing, the capability of implementing externally controlled boundary conditions using the Kestrel Software Development Kit (SDK) is crucially important. Feedback flow control is accomplished in general via sensors in the flow, a controller, and an actuator. A generic 'ComponentX' is provided with the SDK and was modified to implement feedback flow control. In the current implementation, sensor data are provided using the access to grid and solution quantities provided within the SDK through the 'Data Warehouse' infrastructure. [18] The controller can be implemented directly in 'ComponentX'; the output of the controller is then written back to the respective mass flow source boundary condition. While this procedure to set the boundary condition was used for the current simulations, results shown in this paper do not yet utilize the full feedback mechanism; instead, the mass source boundary condition is set to a fixed values. Therefore, the forcing is referred to as 'open-loop' control rather than 'closed-loop' or feedback control. While this type of control could also be achieved using the standard mass flow source boundary condition, it was important to implement it in this manner to test the infrastructure for eventual implementation of feedback control.

The geometry in Fig. 2 was created in Solidworks® and imported into Simcenter SolidMesh. [19] The geometry was completed by a symmetry plane at the wing root and a hemispherical farfield with a radius of 10 times the wing span. The grid spacing on the wing was chosen to match the grids which were developed in the companion paper [20], which includes a spatial and temporal resolution study. The wall normal spacing resulted in $y^+ < 1$ for the whole wing expect inside the blowing ports, where $y^+ < 3$ for the case with blowing; the complete grid had 20.3 million cells. The wing geometry with the grid on the symmetry plane, the wing surface grid and a close-up of the grid at a blowing slot are shown in Fig. 3.

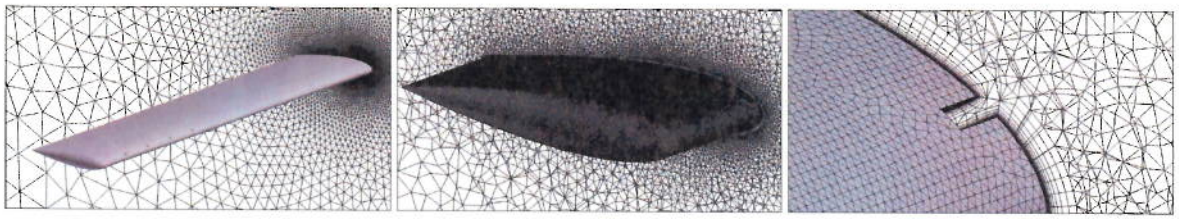

a) NACA0018 Wing b) Surface Mesh c) Blowing Slot

Figure 3. 20.3 million cell grid of the finite aspect ratio NACA0018 wing.

B. Structural Model

To utilize the fluid-structure interaction components within Kestrel, a modal structural model of the geometry is necessary. For the basic problem of a linearly elastic wing, where the material obeys Hooke's Law, the system of equations to be analyzed is a second order ordinary differential equation describing a mass-spring-damper system. This system

can be written, after a Laplace transform, as

$$[Ms^2 + Cs + K]\mathbf{q} = F, \tag{1}$$

where M is the mass matrix, C is the damping matrix, K is the stiffness matrix, $\mathbf{q}$ is the vector of degrees of freedom (6-DoF for each node, i, three translations and three rotations), s is the Laplace variable, and F is the force acting at the nodal location. For practical implementation, the geometry is discretized and a finite element approach; the resulting mass, damping and stiffness matrices are formed and the system of equations are formulated as,

$$\begin{bmatrix} \dot{\mathbf{q}} \\ \ddot{\mathbf{q}} \end{bmatrix} = \begin{bmatrix} 0 & 1 \\ -\frac{K}{M} & -C \end{bmatrix} \begin{bmatrix} \mathbf{q} \\ \dot{\mathbf{q}} \end{bmatrix}, \tag{2}$$

An eigen-analysis of the system of equations results in the eigenvalues, λ_i, and eigenvectors, ϕ_i. The generalized coordinates are then, $\mathbf{n} = \phi\mathbf{q}$. In the case of vibrational analysis, the resonant frequency of the i^{th} eigenvalue becomes $\omega_i = \sqrt{\lambda_i}$. The resulting set of equations are normalized by the mass, such that $\phi^T M\phi = I$. The normalized mass, damping, and stiffness matrices are now diagonal and scaled appropriately. A reduced order model is formulated by truncating the mode set at a desired level, and all of this information is put into an input file (Kestrel .csd file) for the CFD-CSD simulation.

For the purposes of this paper, the simplest structural model was used: the wing material is homogeneous, thus the mass and damping matrices are the identity. The wing structure is modeled by a finite dimensional rectangular beam using brick elements. A finite-element method (FEM) code was employed in MATLAB® to solve for the corresponding eigenvalues and eigenvectors of the linear system. Assuming a linearly elastic material allows for changes to the material properties by simply changing the generalized mass, damping, and stiffness which are part of the eigen solution. In addition, these values are accessible directly in the Kestrel structure input file, which even allows for changes to these values individually for each mode. However, one must be careful to not exceed the deformation limitations imposed by the assumption of a linear model.

C. Open-Loop Forcing

To augment the flow features over the surface of the wing, blowing slots, as shown in Figs. 2 and 3, were integrated along the wing. The base of the slot was set as a source boundary condition such that the magnitude of the mass flow through the patch could be adjusted using the Kestrel SDK features described above. The actuation strength is then governed by the mass flow through the source patch at the base of the forcing slot. To normalize this mass flow with the momentum in the flow, the normalized momentum coefficient, C_μ, is defined as follows,

$$C_\mu = \frac{\int_A \rho \hat{V}(\hat{V} \cdot \hat{n}) dA_{jet}}{\rho_\infty U_\infty^2 A_{ref}}. \tag{3}$$

Because the velocity vector, $\hat{V}$, is set normal to the patch this value becomes the magnitude of the vector, V_{jet}. Also, because exit velocities are strictly less than M $= 0.1$, the velocity at the jet orifice is incompressible; thus, the density is constant throughout the flowfield and can be removed from equation (3). The expression for the momentum coefficient can then be simplified to

$$C_\mu = \frac{V_{jet}^2 A_{jet}}{U_\infty^2 A_{ref}}. \tag{4}$$

The area ratio of the jet orifice ($A_{jet} = 10^{-5}\text{m}^2$) to the reference area ($A_{ref} = 0.06\text{m}^2$) is equal to 1.67×10^{-4}, and the velocity ratio for these preliminary results was chosen such that, $V_{jet} = 0.5U_\infty$, giving a momentum coefficient of $C_\mu = 4.17 \times 10^{-5}$ per slot. Since 4 slots are used, the total momentum being induced into the flow field is $C_\mu = 1.67 \times 10^{-4}$.

III. Results

The results below will be presented in stepwise manner, where the three regimes of fluid-structure interaction as identified in Section I are presented. First, results are shown for the rigid wing for both unforced and open-loop forced simulations. This provides insight to the control efficacy of the blowing ports on the rigid wing. Secondly, the structural model of the NACA0018 is presented which includes spatial modes, stiffness, and resonate frequencies. Finally, the full CFD-CSD simulations are presented which show both unactuated flutter in comparison with the actuated flutter simulation. The efficacy of open-loop control of the fluid-structure interaction problem is investigated using a single actuation amplitude. The resulting forces and deformation of the *unforced* simulation are shown to be different from the *forced* simulation. While not yet conclusive, these results provide a convincing proof of concept at flow control can be used to alter the flow field in a way that changes the structural deformation.

A. Rigid wing

For comparison, the solution for a rigid wing will be presented first. Figure 4 shows the surface pressure in color and surface streamlines. As expected at this angle of attack, the flow is attached and no significant flow structures develop. In Fig. 4b, a close-up of the flow field near the blowing ports is shown. The results indicate that there is a negligible effect of the blowing ports on the flow structures when they are turned off.

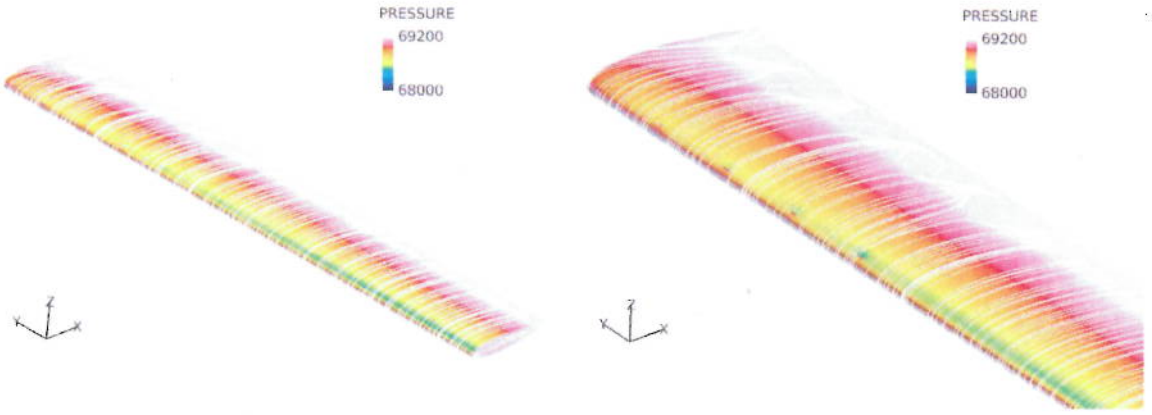

a) Full wing. b) Zoomed view near blowing ports.

Figure 4. Flow field of the undeformed wing, no forcing. Pressure in Pa.

Once the blowing is turned on ($C_\mu = 1.67 \times 10^{-4}$), vortices develop at the blowing slots and travel downstream. Figure 5 shows the flow field for the rigid wing when the blowing slots are activated. The structures are visualized using the Q=0.1 iso-surface. Note that in Fig. 5, the iso-surface is cut-off at x/c=0.5 for visualization purposes. Due to the development of these structures, the surface pressure changes as shown in Fig. 6. Low pressure can now be observed near the blowing slot exits, and the footprint of the structures is visible downstream. As noted earlier, at this angle of attack, the effect of blowing on the rigid wing was expected to be minimal, and the results confirm this assertion. The main purpose of these simulations was to provide a baseline for comparison with the flexible wing.

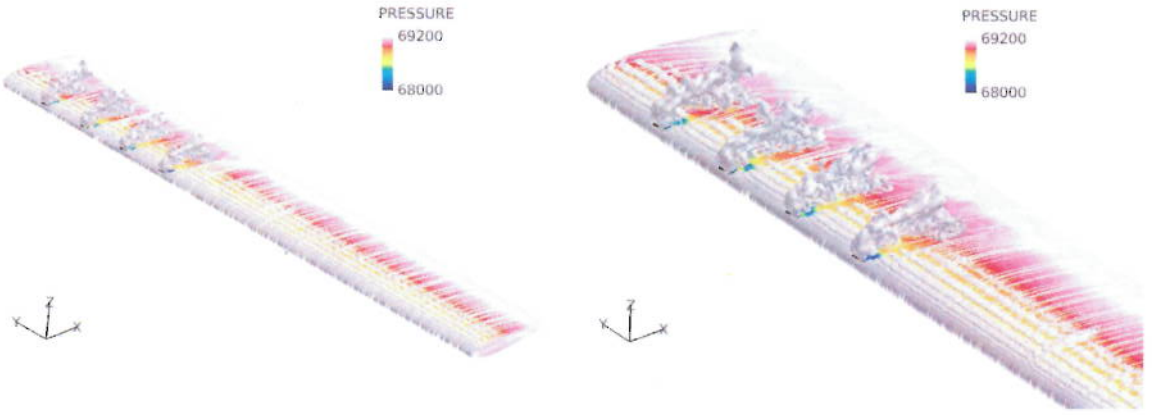

a) Full wing. b) Zoomed view near blowing ports.

Figure 5. Flow field of the undeformed wing, with forcing. Isosurface of normalized Q=0.1. Pressure in Pa.

To compare the effect of blowing on this rigid wing, table 1 summarizes the lift, drag, pitching moment, and roll moment coefficients of the wing without and with blowing. As shown in the table, blowing increases the lift coefficient by approximately 7 percent, which in turn increases the magnitude of the pitching moment and the rolling moment due to the changes in lift occurring in the outboard region of the wing near the leading edge. No measurable effect on the drag coefficient was noted.

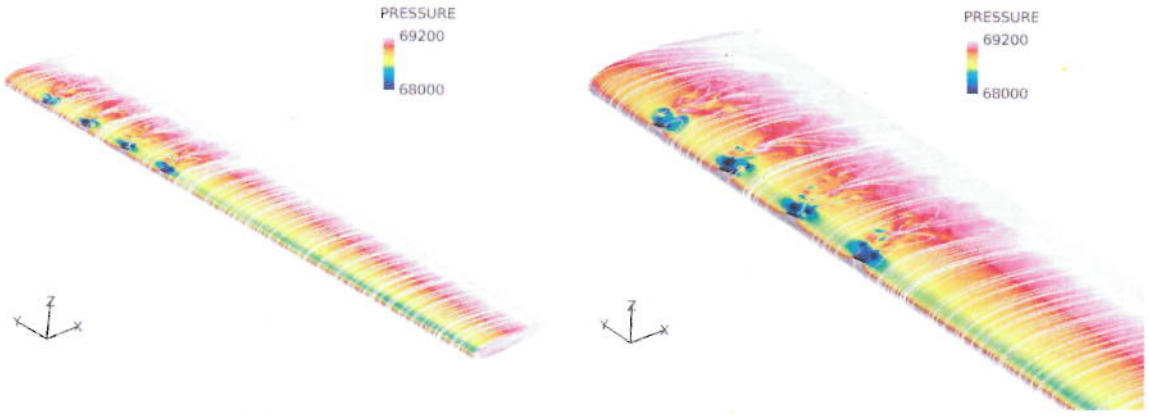

a) Full wing.

b) Zoomed view near blowing ports.

Figure 6. Flow field of the undeformed wing, with forcing. Pressure in Pa.

Table 1. Coefficients for the rigid wing with and without blowing.

C_μ	c_L	c_D	$c_{\mathscr{M}}$	$c_{\mathscr{L}}$
0	0.407	0.025	-0.075	-1.08
1.67×10^{-4}	0.430	0.025	-0.085	-1.18

B. Structural modal deformation

As outlined above, a linear modal model of the structure was developed. The cantilevered NACA0018 wing was assumed to have a rectangular cross section with matching areas for simplicity. For the finite element analysis, beam elements were used with a total of 50 elements discretizing both the chordwise and the spanwise directions. The thickness was discretized by a single element. At this spatial resolution, convergence was achieved and the results matched experimental static deformation measurements and the analytical solutions of the modal frequencies. For the coupled fluid-structure interaction simulations, a 5-mode model was chosen which included the first and second spanwise bending modes (Fig. 7a and 7b), an in-plane bending mode (Fig. 7c), and the first torsional mode (Fig. 7d). The final mode in the model, which contributed negligibly to the deformation, was the third bending mode.

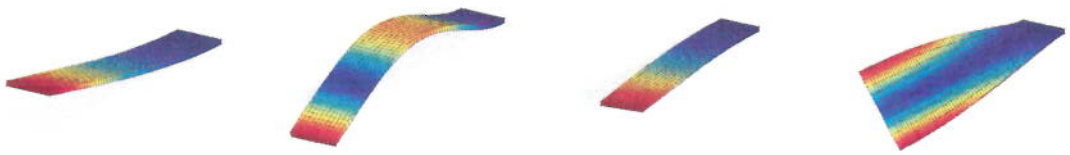

a) First bending mode

b) Second bending mode

c) In-plane bending mode

d) First torsional mode

Figure 7. The first four modes of deformation of the rectangular beam.

The structural parameters of the wing were tailored based on modal parameters to approach a flutter limit cycle oscillation. The damping and torsional rigidity was estimated through a flutter prediction technique and companion experiments to develop a wing structure which naturally oscillated at the given Mach number and dynamic pressure. [20] A summary of the structural parameters is given in Table 2. Note that the bending stiffness is much larger than the torsional stiffness to excite the torsional instability (i.e., a limit cycle oscillation in angle of twist) commonly known as stall flutter as opposed to classical flutter in which the torsional and bending modes couple to produce a pitch-plunge limit cycle oscillation (LCO).

With this structural model, the simulations described above for the rigid wing were repeated for the elastic wing to assess the changes in the forcing effectiveness due to the deformation of the wing.

Table 2. Structural parameters for the aeroelastic simulations.

Bending:	K_h [N/m]	ζ [N/m-s]	m [kg]	$\bar{K}$	freq [hz]
	64412	2.84E-02	0.81	460085	107.9
Torsion:	K_θ [N-m/rad]	η [kg-m-s^2/rad]	J [kg-m^2/rad]	$\bar{K}$	freq [hz]
	2.00	2.84E-02	2.51E-04	7963	14.2

First, the time history of the lift and drag coefficients are plotted in Fig. 8 and the time history of the wing tip twist and bending displacement is shown in Fig. 9. Results for both the unforced ($C_\mu = 0$) and forced ($C_\mu = 1.67 \times 10^{-4}$) aeroelastic simulations are plotted. As shown in Fig. 8a, the oscillations in the lift coefficient are very effectively reduced by the blowing because it induces separation at lower angles of attack than in the unforced case. Interestingly, after the initial transient, as the tip twist reduces due to elastic forces ($t > 0.06$s, see Fig. 9a), the results with blowing show a large reduction in the amplitude of the twist oscillation even though the mean lift coefficients does not seem to be reduced significantly. As observed for the lift coefficient, the drag coefficient obtained from the forced simulation also shows a significant reduction in oscillation amplitude. Finally, in Fig. 9b, the wing tip deflection due to bending shows significant changes as well. In the case of flow control, the initial deflection is slightly reduced, but as the twist angle reduces, the bending deformation oscillates around its new mean at a significantly reduced amplitude and at a frequency that is approximately four times larger than in the unforced case.

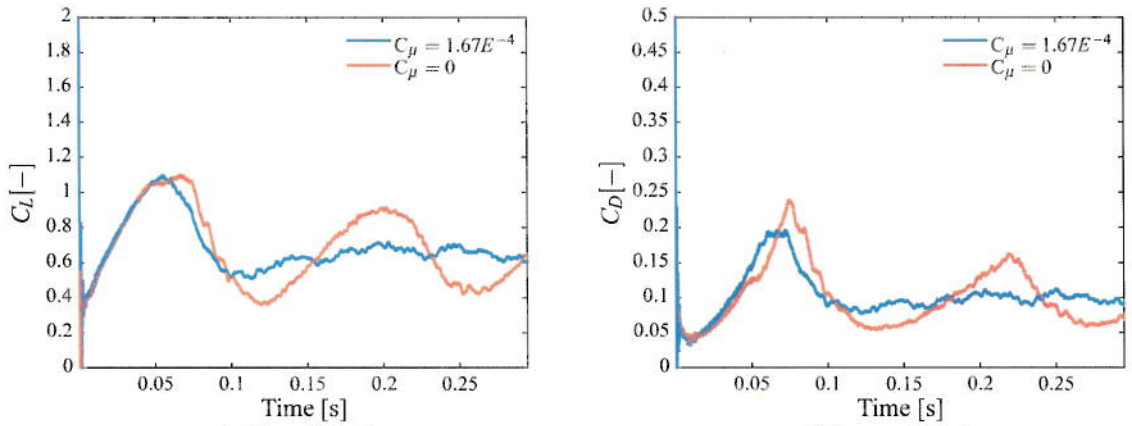

a) Lift coefficient. b) Drag coefficient.

Figure 8. Force coefficients for unforced (red) and forced (blue) simulations.

To better illustrate the effectiveness of blowing on the aeroelastic behavior of the flexible wing, a phase plot is shown in Fig. 10, plotting the lift coefficient against the tip twist angle of the wing. The unactuated case (red) shows an initial transient due to the change from rigid wing to flexible wing. This transient is due to the onset of twist deformation and thus generates more lift. At large enough angle, the flow separates and the elastic forces in the structure reduce the angle of twist. For the unforced simulation, a slightly damped LCO results and an orbit about an equilibrium point is observed. In contrast, the actuated simulation (shown in blue in Fig. 10) displays the same initial transient with a slightly reduced amplitude (see also Fig. 9a). More importantly, the phase plot clearly shows that the actuated wing reaches the equilibrium point much quicker than the unactuated wing. From a dynamical system perspective, the actuation on the flexible wing has increased the overall damping in the aeroelastic behavior.

Figure 11 shows a snapshot of the instantaneous flow field at the end of each run, t=0.3s. As shown in the figure, even in the unforced case, Fig. 11a, the control ports have an effect on the flow field in the outboard section of the wing. The data indicates that the flow field separates further upstream behind the control ports when compared to the inboard section of the wing. In contrast, when blowing is turned on, Fig. 11b, the skin friction coefficient increases significantly locally around the blowing ports, indicating the development of streamwise vortices, which result in attached flow and a slightly higher drag, which may be partially offset by the reduced skin friction inboard of the blowing ports.

When forcing is turned on, the flow structures identified by the Q-criterion (Fig. 13) change significantly from the unforced case. The result of these structures generated by the blowing input is a reduction in lift, increase in

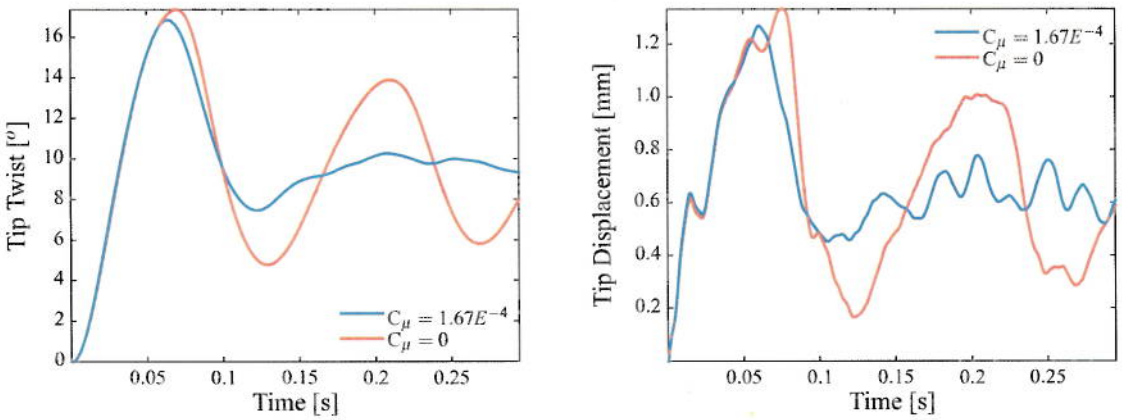

a) Tip displacement. b) Tip twist angle.

Figure 9. Tip deformation for unforced (red) and forced (blue) simulations.

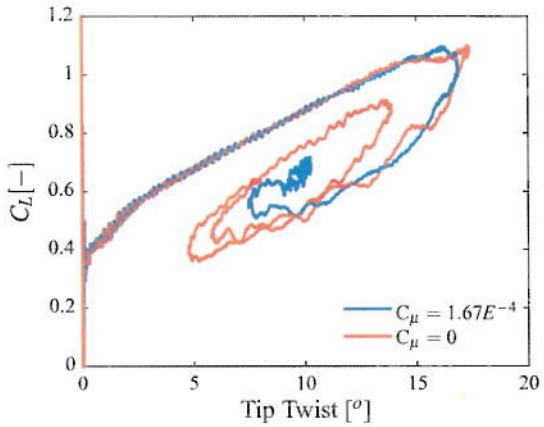

Figure 10. Phase plot of the lift coefficient verse the tip twist for the unforced (green) and forced(blue) simulation.

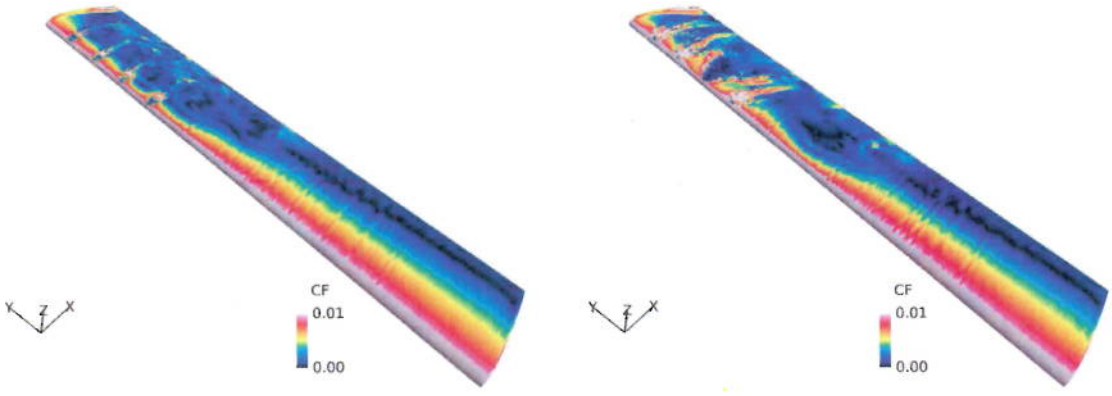

a) Unforced b) Forced

Figure 11. Instantaneous deformed geometry and skin friction coefficient for the unforced simulation. t=0.3s

drag, and a reduction in the magnitude of the rolling moment (see table 3). This is almost a complete reversal of the trends seen for the rigid wing, where blowing increased the lift and the magnitude of the pitching moment and rolling moment. Also note, comparing tables 1 and **??**, that the lift and drag coefficients are significantly higher for the flexible wing; furthermore, the pitching moment is reduced and the rolling moment increased. These dramatic changes in the performance due the flexibility of the wing are not yet fully understood and are currently being investigated.

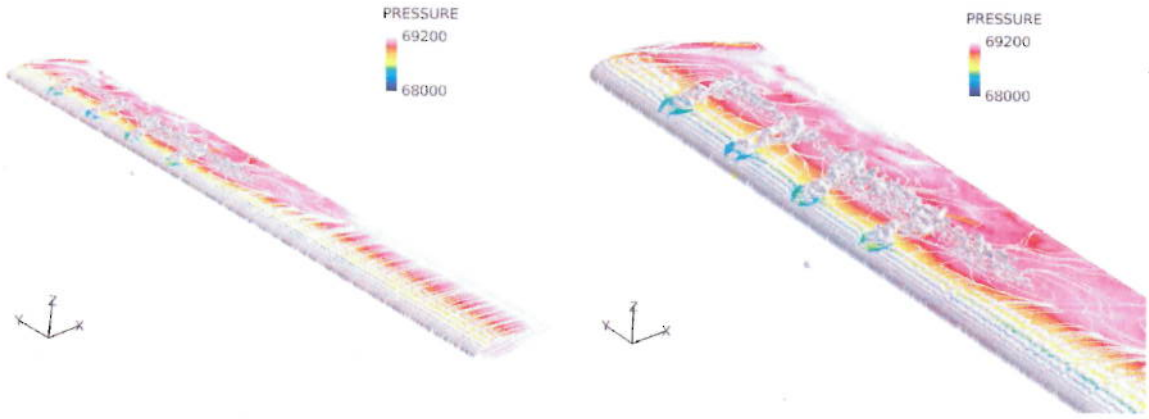

a) Full wing. b) Zoomed view near blowing ports.

Figure 12. Flow field of the deforming wing without blowing.

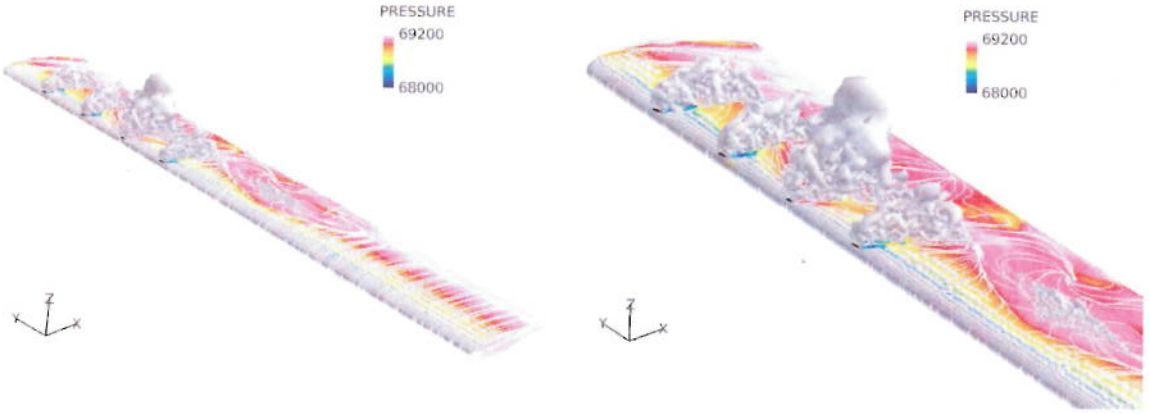

a) Full wing. b) Zoomed view near blowing ports.

Figure 13. Flow field of the deforming wing with active blowing.

Table 3. Coefficients for the flexible wing with and without blowing.

C_μ	c_L	c_D	$c_{\mathscr{M}}$	$c_{\mathscr{L}}$
0	0.635	0.070	-0.014	-1.92
1.67×10^{-4}	0.607	0.092	-0.014	-1.81

IV. Conclusions

In this paper, HPCMP CREATE™-AV Kestrel was used to simulate the flow around a rectangular wing with open-loop flow control (steady blowing). Actuation was introduced through four blowing slots in the outboard section of the wing near the leading edge. To assess the efficacy of flow control to alter the deformation of an aeroelastically soft wing, the flowfield around a rigid wing was compared to the one around the deforming wing. The results indicate that

control by blowing has a pronounced effect on the flowfield and therefore on the aerodynamic coefficients. The lift is increased, as are the pitching and rolling moments.

When aeroelastic deformation is considered, the picture changes significantly. First, the flexible wing showed higher lift and drag due to the increased local angle of attack in the outboard section of the wing. Furthermore, the pitching and rolling moments were significantly reduced. The effect of these changes in the forces and moments on the overall performance of the aeroelastic wing have not been completely analyzed because the time history acquired is too short. Once the aeroelastic wing simulations have reached their dynamic equilibrium, further analysis of the effect of forcing will be performed.

Acknowledgments

The support of the HPCMP CREATE™-AV Kestrel and HPCMP CREATE™–MG Capstone development and quality assurance teams is gratefully acknowledged. Computations were performed through a grant of high-performance computing time from the U.S. Department of Defense High Performance Computing Shared Resource Center at the U.S. Air Force Research Laboratory.

The authors would like to acknowledge funding from Dr. Douglas Smith through the Air Force Office of Scientific Research Flow Control and Interaction portfolio.

This material is based on research sponsored by the US Air Force Academy under agreements number FA7000-13-2-0002 and FA7000-13-2-0009. The U.S. Government is authorized to reproduce and distribute reprints for Governmental purposes notwithstanding any copyright notation thereon.

The views and conclusions contained herein are those of the authors and should not be interpreted as necessarily representing the official policies or endorsements, either expressed or implied, of the US Air Force Academy or the U.S. Government.

References

[1] Hassig, H. J., "An approximate true damping solution of the flutter equation by determinant iteration." *J. Aircraft*, Vol. 8, No. 11, 1971, pp. 885–889.

[2] Chen, P., "Damping perturbation method for flutter solution: the g-method," *AIAA J.*, Vol. 38, No. 9, 2000, pp. 1519–1524.

[3] Ju, Q. and Qin, S., "New Improved g Method for Flutter Solution," *J. Aircraft*, Vol. 46, No. 6, 2009, pp. 2184–2186.

[4] Dowell, E. H. and Hall, K. C., "Modeling of Fluid-Structure Interaction," *Ann. Rev. Fluid Mech.*, Vol. 33, 2001, pp. 445–490.

[5] Beranek, J., Nicolai, L., Buonanno, M., Burnett, E., Atkinson, C., Holm-Hansen, B., and Flick, P., "Conceptual Design of a Multi-utility Aeroelastic Demonstrator," *AIAA Paper 2010-9350*, 2010.

[6] Ryan, J. J., Bosworth, J. T., Burken, J. J., and Suh, P. M., "Current and Future Research in Active Control of Lightweight, Flexible Structures Using the X-56 Aircraft," *AIAA Paper 2014-0597*, 2014.

[7] Fagley, C., Porter, C., and McLaughlin, T., "Predictive Flow Control to Minimize Convective Time Delays," *AIAA Paper 2013-5016*, 2013.

[8] Thomas, R. H., Choudhari, M. M., and Joslin, R. D., "Flow and Noise Control: Review and Assessment of Future Directions," Tech. rep., NASA TM-2002-211631, 2002.

[9] Cattafesta, L. N. and Sheplak, M., "Actuators for Active Flow Control," *Ann. Rev. Fluid Mech.*, Vol. 43, 2011, pp. 247–272.

[10] Morton, S. A., McDaniel, D. R., Sears, D. R., Tillman, B., and Tuckey, T. R., "Kestrel A Fixed Wing Virtual Aircraft Product of the CREATE Program," *AIAA Paper 2009-0338*, 2009.

[11] Morton, S. A., McDaniel, D. R., Sears, D. A., Tillmann, B., and Tuckey, T. R., "Rigid, Maneuvering, and Aeroelastic Results for Kestrel - A CREATE Simulation Tool," *AIAA Paper 2010-1233*, 2010.

[12] Morton, S. A., Lamberson, S. E., , and McDaniel, D. R., "Static and Dynamic Aeroelastic Simulations Using Kestrel - A CREATE Aircraft Simulation Tool," *AIAA Paper 2012-1800*, 2012.

[13] Dean, J. P., Clifton, J. D., Bodkin, D. J., and Ratcliff, J., "High Resolution CFD Simulations of Maneuvering Aircraft Using the CREATE-AV/Kestrel Solver," *AIAA Paper 2011-1109*, 2011.

[14] Spalart, P. and Allmaras, S., "A One-Equation Turbulence Model for Aerodynamic Flows," *Recherche Aerospatiale*, Vol. 1, 1994, pp. 5–21.

[15] Shur, M., Strelets, M., Travin, A., and Spalart, P., "Turbulence Modeling in Rotating and Curved Channels: Assessing the Spalart-Shur Correction," *AIAA J.*, Vol. 38, No. 5, 2000, pp. 784–792.

[16] Menter, F., "Two-Equation Eddy-Viscosity Turbulence Models for Engineering Applications," *AIAA J.*, Vol. 32, No. 8, 1994, pp. 1598–1605.

[17] Spalart, P. R., Deck, S., Shur, M. L., Squires, K. D., Strelets, M. K., and Travin, A., "A new version of detached-eddy simulation, resistant to ambiguous grid densities," *Theor. Comput. Fluid Dyn.*, Vol. 20, 2006, pp. 181–195.

[18] McDaniel, D. R., Tuckey, T. R., and Morton, S. A., "Multiple Bodies, Motion, and Mash-Ups: Handling Complex Use-Cases with Kestrel," *AIAA Paper 2014-0415*, 2014.

[19] Gaither, J., Marcum, D., and Mitchell, B., "Solidmesh: A solid modeling approach to unstructured grid generation," *7th Int. Conf. Numerical Grid Generation in Computational Field Simulations*, 2000.

[20] Fagley, C., Seidel, J., and McLaughlin, T., "Aeroelastic Response of a Finite Span NACA 0018Wing Part 2: Computational Simulations," *AIAA Paper 2015 Pending*, 2015.